# Multi-Mode Transmitter Based on Silicon Microring Modulators

Mengyuan Ye, Yunlong Li, Weilun Zhang, Li Liu, Yang Shi, and Yu Yu, *Member, IEEE*

***Abstract*—We propose and demonstrate a multi-mode transmitter based on cascaded silicon microring modulators (MRMs). By sharing bus waveguide at drop ports of the MRMs, data modulation and mode multiplexing could be achieved simultaneously, resulting in a simplified layout with compact size. For the proof-of-concept demonstration, multi-mode transmitter for $TE_0$ and $TE_1$ modes is fabricated. Transmission of non-return-to-zero on-off keying (NRZ-OOK) signals with the bit rate of 2 × 25 Gbps is experimentally demonstrated. Measured eye diagrams and bit error rate (BER) results indicate good transmission performance.**

***Index Terms*—Mode multiplexing, microring modulators, transmitter.**

## I. Introduction

With the rapid development of new technologies such as 4K media, 5G and artificial intelligence, short-reach transmitter with large capacity, compact footprint and low-cost is highly desired nowadays [1]. Silicon photonics is commonly regarded as a promising solution for data-center transmitters due to its advantages as low-cost, strong mode confinement and compatibility with matured Complementary Metal Oxide Semiconductor (CMOS) technologies [1]–[3]. As the data capacity of silicon transmitter depends significantly on the modulator bandwidth, silicon integrated modulators have been investigated extensively in the past decade [4]–[6].

To further increase the data capacity of silicon transmitter, wavelength division multiplexing (WDM) technology has been widely studied [7]–[11]. Among all kinds of techniques, transmitter based on cascaded MRMs demonstrated an elegant way to achieve both large bandwidth and small footprint by sharing the bus waveguide for different wavelengths [11]–[15]. However, silicon transmitter based on WDM technique meets its bottleneck for the on-chip applications due to multiple laser sources on silicon platform being hard to realize and difficult to manage [16]. Alternatively, mode division multiplexing (MDM) technique attracts more and more attention by introducing high-order modes to further enlarge the transmission capacity [17]–[19]. Thus, single laser multi-mode transmitter with large data capacity could be achieved. In addition, as the MDM techniques are compatible with the existing WDM and polarization division multiplexing (PDM) technologies [19], [20], the data capacity is expected to be further increased by combining multi-mode transmitter with other multiplexing technologies.

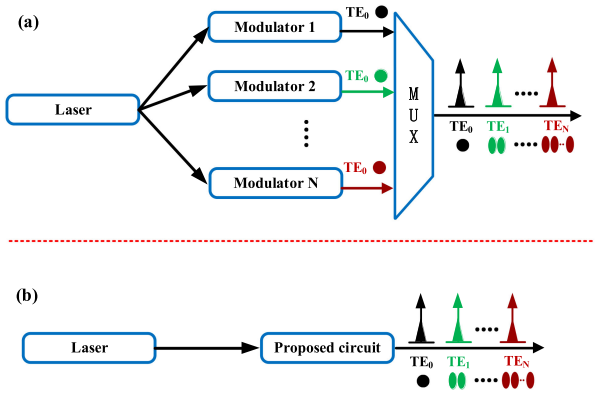


Fig. 1. (a) Conventional architecture of multi-mode transmitter; (b) architecture utilizing the proposed scheme.

Conventional architecture of multi-mode transmitter is shown in Fig. 1(a). Due to modulators can only deal with single-mode signals, N single-mode modulators and a mode MUX are commonly needed to build up a multi-mode transmitter, resulting in a complex and inefficient layout. In recent years, architecture which could process multi-mode signals simultaneously attracts more and more attention [21]–[27]. Reference [26] proposed and demonstrated an integrated multimode switch which can simultaneously process on different wavelengths and modes. In our previous work [27], a silicon multi-mode ring resonator supporting four modes had been demonstrated.

In this paper, we propose and demonstrate an integrated multi-mode transmitter based on cascaded silicon MRMs. Architecture of the proposed circuit is shown in Fig. 1(b). Data modulation and mode multiplexing could be processed simultaneously in the proposed circuit, achieving simple architecture with compact size. For the proof-of-concept demonstration, multi-mode transmitter for $TE_0$ and $TE_1$ modes is fabricated. Transmission of non-return-to-zero on-off keying (NRZ-OOK) signals with the bit rate of 2 × 25 Gbps is experimentally demonstrated. Measured eye diagrams and bit error rate (BER) results indicate good transmission performance.

Manuscript received 9 June 2022; revised 3 July 2022; accepted 5 July 2022. Date of publication 8 July 2022; date of current version 18 July 2022. This work was supported by the National Natural Science Foundation of China under Grants 61911530161 and 62175220. *(Corresponding author: Li Liu.)*

Mengyuan Ye, Yunlong Li, Weilun Zhang, and Li Liu are with the School of Automation, China University of Geosciences, Wuhan 430074, China, and also with the Hubei Key Laboratory of Advanced Control and Intelligent Automation for Complex Systems, Wuhan 430074, China (e-mail: yemy@cug.edu.cn; liyunlong@cug.edu.cn; weilun@cug.edu.cn; liliu@cug.edu.cn).

Yang Shi and Yu Yu are with the Wuhan National Laboratory for Optoelectronics, Huazhong University of Science and Technology, Wuhan 430074, China (e-mail: d201980780@hust.edu.cn; yuyu@mail.hust.edu.cn).

Digital Object Identifier 10.1109/JPHOT.2022.3189438

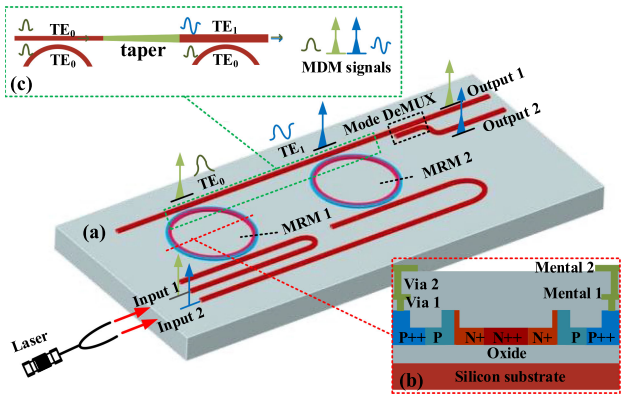


Fig. 2. (a) Schematics of the proposed multi-mode transmitter; (b) cross-section of the MRM and (c) schematics of the MDM signals generation.

## II. Design and Fabrication

Schematic of the proposed multi-mode transmitter is shown in Fig. 2(a). The circuit consists of two cascaded MRMs with both through and drop ports. Continuous-wave (CW) light from the laser source is launched into the Input ports, and coupled into the cascaded MRMs, in which two separate signals could be modulated. Fig. 2(b) shows the cross-section of those MRMs.

To generate MDM signals at output of the circuit, additional mode MUX is commonly needed, as Fig. 1(a) shows. Here MDM signals generation without mode MUX could be achieved by sharing one bus waveguide at drop ports of both MRMs. The proposed scheme is shown in Fig. 2(c). Ring bend waveguides of both MRMs and drop port waveguide of MRM1 are set to be single-mode, while drop port waveguide of MRM2 is specifically designed to satisfy the phase matching condition between $TE_0$ of ring bend waveguide and $TE_1$ mode of drop port waveguide. In addition, a taper is utilized to connect the waveguides with different widths, achieving adiabatic $TE_0$ mode signal transmission. Thus signal modulation and mode multiplexing could be processed simultaneously. To be noted, such design could be further scalable to higher order modes by just varying the waveguide width of drop port. In order to experimentally evaluate performance of the proposed circuit, extra mode DeMUX structure is designed to perform mode de-multiplexing for output signals.

The proposed circuit is designed and fabricated based on the silicon-on-insulator (SOI) wafer with top silicon layer of 220 nm and SiO2 layer of 2 $\mu$m. 248 nm deep ultraviolet photolithography and inductively coupled plasma (ICP) etching are used to form the waveguide structure. The etching depth of the ridge waveguide is 130 nm. The widths of single-mode waveguide are chosen as 500 nm, while the multimode waveguide is designed as 1.1 $\mu$m to satisfy the phase matching condition of $TE_0$-$TE_1$ mode conversion. The length of the adiabatic tapers is set as 180 $\mu$m. The radius and gap of the MRRs are chosen to be 20 $\mu$m and 280 nm, respectively. The nominal doping concentrations of the P-dopant and $N^+$-dopant are $5 \times 10^{17} cm^{-3}$ and $3 \times 10^{18} cm^{-3}$, respectively. Termination and capacitance of the MRM are calculated to be 50 ohm and 28 fF, respectively. To adjust the resonance wavelength of the MRR, an integrated TiN heater is fabricated on top of the MRMs. Thickness and width of the heater are 200 nm and 5 $\mu$m, respectively. Insertion loss of the mode DeMUX for $TE_0$ and $TE_1$ mode is measured to be 0.3 dB and 0.6 dB, respectively. While mode crosstalk is measured to be $<-20$ dB within C-band. The circuit is fabricated at the Advanced Micro Foundry (AMF) in Singapore. Microscope image of the fabricated device is illustrated in Fig. 3. In order to get a quantitative study of the impact between two modulated data-streams, two input port were utilized in the layout design.

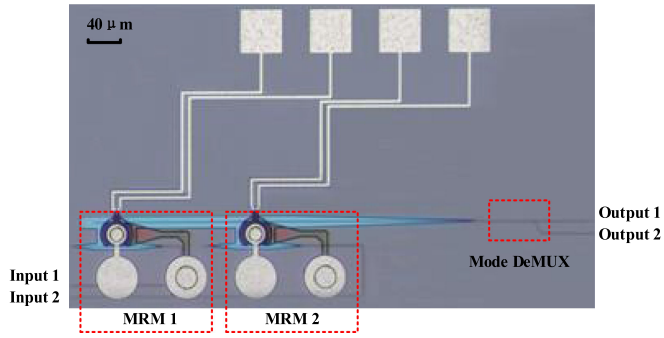


Fig. 3. Microscope image of the fabricated device.

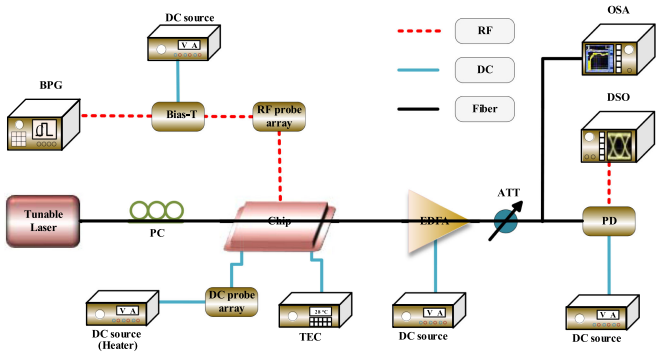


Fig. 4. Experimental setup. (DC: Direct Current, RF: Radio Frequency, PC: Polarization Controller, BPG: Bit Pattern Generator, OSA: Optical Spectrum Analyzer, DSO: Digital Sampling Oscilloscope, EDFA: Erbium Doped Fiber Application Amplifier, ATT: Attenuator, TEC: Temperature Electrical Controller, Amplifier: broadband Amplifier).

## III. Experiments

In order to characterize performance of the fabricated circuit, both transmission spectra measurement and high-speed signal transmission test are performed. Experimental setup is shown in Fig. 4. A tunable laser is used as the light source. The laser relative intensity noise (RIN) is $\sim -145$ dB/Hz. The following Polarization Controller (PC) is used to assist with polarization adjustment. The chip is set on stage with Temperature Electrical Controller (TEC) under it, which helps to avoid environmental influence. Direct Current (DC) probe array is used for the resonant wavelength adjustment, while Radio Frequency (RF) probe array is used to transfer RF signal from the Bit Pattern Generator (BPG) to the MRMs. Erbium Doped Fiber Application Amplifier (EDFA) and Attenuator (ATT) are used to optimize the output power for a fair comparison.

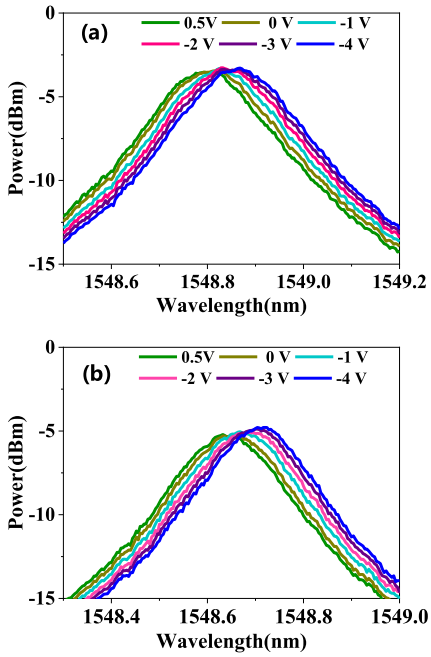


Fig. 5. Measured spectra with different DC bias of (a) MRM1 and (b) MRM2.

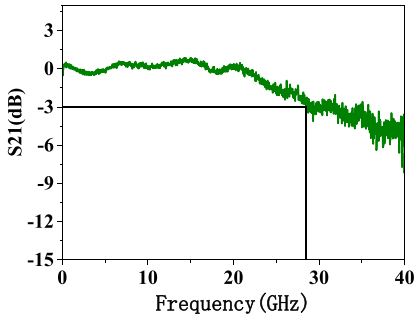


Fig. 6. Measured S21 curve of the MRM.

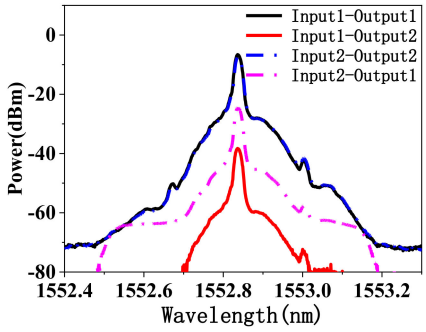


Fig. 7. spectra for different combinations of inputs and outputs.

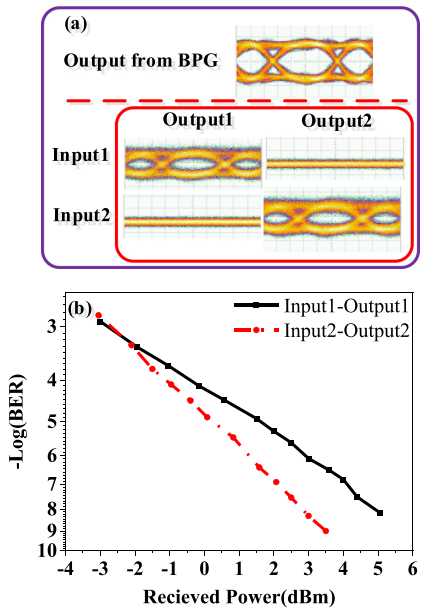


Fig. 8. (a) Measured eye diagrams; (b) The BER measurement results.

## IV. Results and Discussion

Fig. 5 shows the measured spectra of both MRMs with different DC bias. It can be seen that the extinction ratio (ER) of both MRMs is >20 dB. Insertion loss of MRM1 and MRM2 are 3.6 dB and 5.2 dB, respectively. Modulation efficiencies of MRM1 and MRM2 are measured to be 16.6 pm/V and 18.2 pm/V respectively, indicating similar modulation efficiency for both modes within bias voltage ranging from between 0.5 to −4V.

To demonstrate the capability of high-speed signal modulation, small signal S21 response of the MRM is also performed. MRM with the same structure parameter is fabricated as reference. S21 measurement is performed by utilizing the vector network analyzer (VNA) and a calibrated high-speed photodetector. The measured amplitude response is illustrated in Fig. 6. A bias-T combined the RF signal and the DC bias was set to be −3V. Wavelength detuning of the MRM was set to be 110 pm on blue-side relative to the resonance. The 3 dB bandwidth is measured to be ∼28GHz.

The NRZ-OOK signal at 25 Gb/s is used to further test the fabricated circuit. In order to characterize the performance conveniently, individual data input has been utilized. Fig. 7 shows the measured spectra for different combination of inputs and outputs. Input1-Output1 and Input2-Output2 represent the case of $TE_0$ and $TE_1$ mode transmission, respectively, while Input1-Output2 and Input2-Output1 represent the case of mode crosstalk. It can be seen that the NRZ-OOK signals are modulated successfully while the mode crosstalk is <20 dB.

Fig. 8(a) shows the measured eye diagrams of signals from both Output1 and Output2, using Input1 and Input2, respectively. Clear and open eyes can be obtained at one output port while signal from the other output port can be barely detected. Extinction Ratios (ERs) of $TE_0$ and $TE_1$ mode are measured to be 1.9 dB and 2 dB, respectively. While the Optic Modulation Amplitudes (OMAs) of the signals are 4.02 mW ($TE_0$) and 4.2 mW ($TE_1$), respectively. Performance of the MRM can be improved by increasing the quality factor, for example, by reducing the coupling to make the transmission notch narrower. The BER measurements are further performed, with results being plotted

in Fig. 8(b). The variation of power penalty between $TE_1$ and $TE_0$ mode transmission is less than 1.5 dB, indicating a good performance of the proposed circuit.

## V. Conclusion

We propose and demonstrate an integrated multi-mode transmitter based on cascaded silicon MRMs. Data modulation and mode multiplexing could be processed simultaneously in the proposed circuit, achieving simple architecture with compact size. For the proof-of-concept demonstration, multi-mode transmitter for $TE_0$ and $TE_1$ modes is fabricated. Transmission of NRZ-OOK signals with the bit rate of $2 \times 25$ Gbps is experimentally demonstrated. Experimental results indicate good performance of the fabricated circuit.

## References


[1] W. Shi, Y. Tian, and A. Gervais, "Scaling capacity of fiber-optic transmission systems via silicon photonics," *Nanophotonics*, vol. 19, no. 16, pp. 4629–4633, 2020.

[2] S. Y. Siew *et al.*, "Review of silicon photonics technology and platform development," *J. Lightw. Technol.*, vol. 39, no. 13, pp. 4374–4389, Jul. 2021.

[3] H. Li *et al.*, "A 112 Gb/s PAM4 silicon photonics transmitter with microring modulator and CMOS driver," *J. Lightw. Technol.*, vol. 38, no. 1, pp. 131–138, Jan. 2020.

[4] G. T. Reed, G. Mashanovich, F. Y. Gardes, and D. J. Thomson, "Silicon optical modulators," *Nature Photon.*, vol. 4, pp. 518–526, Jul. 2010.

[5] A. Rahim *et al.*, "Taking silicon photonics modulators to a higher performance level: State-of-the-art and a review of new technologies," *Adv. Photon.*, vol. 3, no. 2, Apr. 2021, Art. no. 024003.

[6] W. Zhang *et al.*, "High bandwidth capacitance efficient silicon MOS modulator," *J. Lightw. Technol.*, vol. 39, no. 1, pp. 201–207, Jan. 2021.

[7] S. Pitris *et al.*, "400 Gb/s silicon photonic transmitter and routing WDM technologies for glueless 8-socket chip-to-chip interconnects," *J. Lightw. Technol.*, vol. 38, no. 13, pp. 3366–3375, Jul. 2020.

[8] C. Li *et al.*, "Hybrid WDM-MDM transmitter with an integrated si modulator array and a micro-resonator comb source," *Opt. Exp.*, vol. 29, no. 24, pp. 39847–39858, 2021.

[9] S. Pitris *et al.*, "O-band silicon photonic transmitters for datacom and computercom interconnects," *J. Lightw. Technol.*, vol. 37, no. 19, pp. 5140–5148, Oct. 2019.

[10] P. Dong, "Silicon photonic integrated circuits for wavelength-division multiplexing applications," *IEEE J. Sel. Top. Quantum Electron.*, vol. 22, no. 6, pp. 370–378, Nov./Dec. 2016.

[11] R. Ding *et al.*, "A compact low-power 320-Gb/s WDM transmitter based on silicon microrings," *IEEE Photon. J.*, vol. 6, no. 3, Jun. 2014, Art. no. 6600608.

[12] Y. Xu *et al.*, "Integrated flexible-grid WDM transmitter using an optical frequency comb in microring modulators," *Opt. Lett.*, vol. 43, no. 7, pp. 1554–1557, 2018.

[13] D. Kong *et al.*, "Intra-datacenter interconnects with a serialized silicon optical frequency comb modulator," *J. Lightw. Technol.*, vol. 38, no. 17, pp. 4677–4682, Sep. 2020.

[14] Y. Xu, J. Lin, R. Dubé-Demers, S. LaRochelle, L. Rusch, and W. Shi, "A single-laser flexible-grid WDM silicon photonic transmitter using microring modulators," in *Proc. Opt. Fiber Commun. Conf.*, 2018, Art. no. W1I.3.

[15] R. Dubé-Demers, S. LaRochelle, and W. Shi, "Low-power DAC-less PAM-4 transmitter using a cascaded microring modulator," *Opt. Lett.*, vol. 41, no. 22, pp. 5369–5372, Nov. 2016.

[16] S. Fathololoumi *et al.*, "1.6 Tbps silicon photonics integrated circuit and 800 Gbps photonic engine for switch co-packaging demonstration," *J. Lightw. Technol.*, vol. 39, no. 4, pp. 1155–1161, Feb. 2021.

[17] X. Wu, C. Huang, K. Xu, W. Zhou, C. Shu, and H. K. Tsang, "$3\times104$ Gb/s single-$\lambda$ interconnect of mode-division multiplexed network with a multicore fiber," *J. Lightw. Technol.*, vol. 36, no. 2, pp. 318–324, Jan. 2018.

[18] L.-W. Luo *et al.*, "WDM-compatible mode-division multiplexing on a silicon chip," *Nature Commun.*, vol. 5, 2014, Art, no. 3069.

[19] Z. Wu *et al.*, "$3 \times 4 \times 10$-Gb/s MDM-WDM transmission over 21-km OM3 MMF with OOK modulation and direct detection," in *Proc. Opt. Fiber Commun.*, 2018, Art. no. W4J.3.

[20] D. Dai *et al.*, "10-channel mode (de)multiplexer with dual polarizations," *Laser Photon. Rev.*, vol. 12, no. 1, Jan. 2018, Art. no. 1700109.

[21] K. Igarashi *et al.*, "Ultra-dense spatial-division-multiplexed optical fiber transmission over 6-mode 19-core fibers," *Opt. Exp.*, vol. 24, no. 10, pp. 10213–10231, 2016.

[22] C. Sun, Y. Yu, and X. Zhang, "Ultra-compact waveguide crossing for a mode-division multiplexing optical network," *Opt. Lett.*, vol. 42, no. 23, pp. 4913–4916, Dec. 2017.

[23] Y. Wang and D. Dai, "Multimode silicon photonic waveguide corner-bend," *Opt. Exp.*, vol. 28, no. 7, pp. 9062–9071, 2020.

[24] L. H. Gabrielli, D. Liu, S. G. Johnson, and M. Lipson, "On-chip transformation optics for multimode waveguide bends," *Nature Commun.*, vol. 3, Nov. 2012, Art. no. 1217.

[25] C. Sun *et al.*, "De-multiplexing free on-chip low-loss multimode switch enabling reconfigurable inter-mode and inter-path routing," *Nanophotonics*, vol. 7, no. 9, pp. 1571–1580, Jul. 2018.

[26] L. Yang *et al.*, "General architectures for on-chip optical space and mode switching," *Optica*, vol. 5, no. 2, pp. 180–187, Feb. 2018.

[27] M. Ye, C. Sun, Y. Yu, Y. Ding, and X. Zhang, "Silicon integrated multimode ring resonator," *Nanophotonics*, vol. 10, no. 4, pp. 1265–1272, Jan. 2021.